Intelligence 66 (2018) 54–63

Contents lists available at ScienceDirect

Intelligence

journal homepage: www.elsevier.com/locate/intell

Delta-gamma coupling as a potential neurophysiological mechanism of fluid intelligence

A. Gągol[a], M. Magnuski[a,b], B. Kroczek[c], P. Kałamała[d], M. Ociepka[c], E. Santarnecchi[e,1], A. Chuderski[a,*,1]

[a] Institute of Philosophy, Jagiellonian University, Grodzka 52, Kraków 31-044, Poland
[b] Department of Psychology, University of Social Sciences and Humanities, Chodakowska 19/31, 03-815 Warsaw, Poland
[c] Institute of Computer Science and Computational Mathematics, Jagiellonian University, Łojasiewicza 6, 30-348 Kraków, Poland
[d] Institute of Psychology, Jagiellonian University, Ingardena 6, 30-060 Kraków, Poland
[e] Berenson-Allen Center for Non-Invasive Brain Stimulation, Beth Israel Deaconess Medical Center, Cognitive Neurology Department, Harvard Medical School, 330 Brookline Ave, Boston, MA 02215, USA

ARTICLE INFO

Keywords:
Fluid intelligence
Cross-frequency coupling
Phase-amplitude coupling
EEG

ABSTRACT

Electrophysiological investigations have pointed out significant yet weak correlations between intelligence and oscillatory brain activity, including the spectral power, frequency, complexity, synchrony, and coherence of electroencephalographic (EEG) signals, however neglecting the interplay between fast and slow neuronal oscillations underlying information transfer in the brain. We found that fluid intelligence level (*gf*) depends on the precise synchronization of fast oscillations to a specific time window of slow brain rhythms. Specifically, by examining EEG recordings of 50 people in resting state as well as during performance at two *gf* tasks we found converging evidence that high-*gf* participants display stronger Phase-Amplitude Coupling (PAC) related to an increased concentration of gamma (~36 Hz) spectral power at the descending phase of delta oscillations (~3 Hz). Delta-gamma PAC strength explained 35% variance in scores on multiple *gf* tests, outperforming six alternative EEG-based predictors including spectral power, complexity and amplitude-amplitude coupling. Present results suggest PAC as a neurophysiological substrate of *gf* in humans, offering novel insight about the role of slow and fast brain rhytms in high-order cognition, as well as a potential new target for neuromodulatory interventions in the healthy and pathological brain.

1. Introduction

Academic and professional success, socio-economic status, and even longevity are all strongly predicted by individual level of psychometric intelligence (Deary, 2012). A key component of intelligence is called fluid intelligence (*gf*), and is assessed as the ability to solve novel problems via abstract reasoning, regardless of prior knowledge and domain-specific skills (McGrew, 2009). Because performance in multiple cognitive domains, including linguistic and mathematical abilities, learning, self-control, and even social skills are strongly correlated with *gf*, decades of research were devoted to understanding the neuronal mechanisms underlying inter-individual differences in *gf* (Colom, Karama, Jung, & Haier, 2010; Deary, Penke, & Johnson, 2010). Multiple neurobiological factors that predict *gf* were found, including structural properties of the neocortex (e.g., Barbey, Colom, Paul, & Grafman, 2014; Basten, Hilger, & Fiebach, 2015; Colom et al., 2009, 2013), integrity of subcortical fiber tracts (e.g., Clayden et al., 2012; Jung & Haier, 2007; Othani et al., 2014; Pineda-Pardo, Martinez, Roman, & Colom, 2016), brain efficiency (e.g., van den Heuvel, Stam, Kahn, & Pol, 2009; Pineda-Pardo et al., 2016), metabolic levels in fronto-parietal regions (e.g., Basten et al., 2015; Dunst et al., 2014; Neubauer & Fink, 2009; Santarnecchi et al., 2017), and organization of spontaneous functional brain activity (e.g., Cole, Yarkoni, Repovs, Anticevic, & Braver, 2012; Finn et al., 2015; Santarnecchi et al., 2015; Schultz & Cole, 2016).

However, each factor explain no more than 25% of interindividual variance in *gf*, and it is not clear how most of those neurobiological factors actually contribute to more effective cognitive performance of high-*gf* individuals. For example, no theory actually provides a quantitative explanation of why and how, for instance, more gray matter in the neocortex and higher integrity of white matter tracts should translate into more valid abstract reasoning in complex cognitive tasks,

* Corresponding author.
E-mail address: Adam.Chuderski@uj.edu.pl (A. Chuderski).
[1] Both authors contributed equally.

https://doi.org/10.1016/j.intell.2017.11.003
Received 15 July 2017; Received in revised form 8 November 2017; Accepted 8 November 2017
Available online 23 November 2017

even though intuitive explanations might be drawn. Also, the relationship between metabolic efficiency during a cognitive task and intelligence is complex, adaptive (Dunst et al., 2014), and whether intelligent brains display lower or higher metabolism depends on many moderators, e.g. the task itself, its relative difficulty, instruction, sex and expertise (Neubauer & Fink, 2009). Finally, brain connectivity studies diverge on whether intelligence is related to either single, local hubs (Cole et al., 2012) or to distributed, global properties (Santarnecchi et al., 2015; van den Heuvel et al., 2009).

By contrast, information-processing theories explain abstract reasoning in terms of effective maintenance, control, and transformation of task-relevant mental structures in the working memory system (e.g., Carpenter, Just, & Shell, 1990; Johnson-Laird, 2006; Ragni & Knauff, 2013). Information within this system is highly accessible, but its duration and capacity are limited (Cowan, 2001). Numerous studies suggest that working memory capacity explains at least 50% of variance in *gf* (e.g., Chuderski, 2013; Kane, Hambrick, & Conway, 2005), being its strongest predictor thus far. However, working memory is a construct not so much simpler than *gf* itself, thus it is not easy to link its capacity to neurophysiology of the human brain. A growing number of primate studies (e.g., Naya & Suzuki, 2011; Siegel, Warden, & Miller, 2009) are showing how information encoding during working memory performance may be underpinned by patterns of both synchronous and asynchronous neuronal oscillations. The role of oscillatory patterns for working memory capacity has been also suggested by intracranial recordings from epileptic patients (e.g., Axmacher et al., 2010; Leszczynski, Fell, & Axmacher, 2015; van Vugt, Schulze-Bonhage, Litt, Brandt, & Kahana, 2010). Such oscillations are also key mechanism in leading neurocomputational models of working memory (e.g., Horn & Usher, 1991; Lisman & Idiart, 1995; Vogel, Woodman, & Luck, 2001) and reasoning (e.g., Eliasmith et al., 2012; Knowlton, Morrison, Hummel, & Holyoak, 2012), which thus link cognitive performance with the interplay between brain oscillatory patterns. In line with this research, our own model (Chuderski & Andrelczyk, 2015) assumed that cross-frequency coupling (CFC) between slow and fast brain oscillations underlying storage and control of information in working memory might play a pivotal role in individual differences in abstract reasoning, and thus might strongly predict *gf*. The goal of the present study was to examine this prediction using electroencephalography (EEG) data collected during *gf* problem-solving in healthy participants.

CFC is considered the optimal coding scheme supporting local and distant information transfer in the human brain (Canolty et al., 2006; Jensen & Colgin, 2007). Specifically, the phase-amplitude modulation of high-frequency electrical activity in the beta (2^4–2^5 Hz) or gamma bands (2^5–2^8 Hz) by the phase of low-frequency delta (2^1–2^2 Hz), theta (2^2–2^3 Hz), or alpha rhythms (2^3–2^4 Hz), observed in electrocorticographic (ECoG) as well as electroencephalographic (EEG) data, has been shown to underpin performance in multiple perceptual, attentional, and memory tasks (Canolty & Knight, 2010; Lisman & Jensen, 2013). For instance, stronger theta/delta modulation of gamma band activity in a spatial cuing task improves focused attention (Szczepanski et al., 2014), while bursts of gamma activity at different phase of the delta cycle seems to reflect mental representation of different categories of objects (faces, scenes, houses, or tools; Watrous, Deuker, Fell, & Axmacher, 2015).

Although several ECoG (e.g., Axmacher et al., 2010; Leszczynski et al., 2015) and EEG studies (e.g., Sauseng et al., 2009) indicated that working capacity may depend on the interplay between amplitude of gamma activity and the phase of theta/alpha, and an EEG study has suggested a weak negative link between resting-state theta-gamma amplitude-amplitude coupling (AAC) and intelligence (Pahor & Jaušovec, 2014b), no study to date has investigated the role of PAC during *gf*-related problem-solving. The present study aimed at the comprehensive investigation of relationships between PAC present in EEG data and *gf*, the latter assessed by the scores on multiple abstract reasoning tests. Specifically, our goal was to identify specific frequencies (if any) involved in PAC, which would most strongly contribute to *gf*. As to date several other EEG-based neurophysiological markers were associated with intelligence, we also aimed to compare the potential contribution of PAC to *gf* to the contribution of these alternative markers.

2. Materials and methods

2.1. Participants

We recruited 33 women and 24 men via internet adverts. For one three-hour session, participants were paid the equivalent of 10 euro in local currency. Mean age was 22.3 years (SD = 2.8, range 19–35). Participants were screened for normal or corrected-to-normal vision and no history of neurological problems, and informed that they could interrupt the data collection and exit the study at any moment. They signed a written consent to participate. Each participant was tested in soundproof, dimly-lit cabin, under the supervision of an experimenter. The study conformed to ethical guidelines of National Science Center of Poland: http://www.ncn.gov.pl/sites/default/files/pliki/2016_zalecenia_Rady_NCN_dot_etyki_badan.pdf, as well as fully conformed to Declaration of Helsinki. Because of either low quality of electroencephalographic (EEG) signal or procedural errors during signal recording, the data from 7 participants had to be discarded from analysis, leading to a final sample of 50 people.

2.2. EEG procedure

First, continuous resting EEG was recorded for 180 s with eyes open and 180 s with eyes closed (Fig. 1). Only eyes closed data was submitted to analysis (henceforth called *Rest* condition). Next, participants performed a computerized variant of Raven's Advanced Progressive

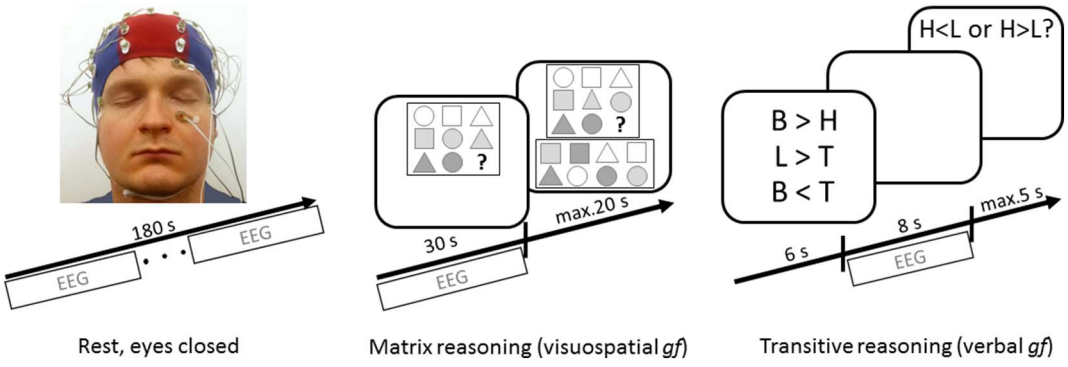

Fig. 1. Experimental design. EEG was recorded both during resting-state and during the solution of two tasks assessing visuospatial and verbal *gf* performance. For additional information see the method section of the paper.

Matrices (*RAPM*) – the gold standard for *gf* testing, consisting of 36 items composed by a three-by-three matrix of geometrical stimuli where the bottom-right stimuli is missing. The task is to identify the relationship between the eight available stimuli and infer the missing one among eight possible alternative solutions. Items difficulty progressed throughout the test. In each of 34 test trials (two easiest items were used for training), the matrix without the eight response options was presented for 30 s, then it was shown together with the potential solutions for additional 20 s, during which the response could be made by indicating the selected answer using a mouse. This two-steps presentation was aimed at eliciting problem solving based on available stimuli, instead of a trial-and-error process focused on testing the different available solutions. Only the EEG signal from the first 30 s was analyzed. After a short break, the participants performed a computerized verbal *gf* test (*Transitive*). The task was to infer the transitive relation between four letters. Each of 34 test trials (and 4 training trials) consisted of three events. First, three pairs of letters, each linked by a relation "larger than" (>) or "smaller than" (<), were shown at the center of the screen for 6 s. The pairs (e.g., "T > H", "L > B", "T < B") always yielded the univocal order ("H < T < B < L"). Next, the stimuli disappeared for 8 s. The EEG signal during this time window, i.e. when participants had to actively maintain the information about the hierarchy, was analyzed. Finally, two alternative, new relations based on the previosuly presented stimuli were shown ("L < H" vs. "L > H"), and participants had 5 s to select the only correct response by a button press (see Fig. 1).

The EEG signal was recorded at 256 Hz from 64 Ag/AgCl scalp electrodes, positioned at the standard 10–20 locations, mounted in an elastic cap, using the Biosemi Active Two recording system. In order to decrease the noise and muscular artifacts, all analyses used signals from only 34 medial electrodes (Fp1, Fpz, Fp2, AF4, AFz, AF3, F3, F1, Fz, F2, F4, FC4, FC2, FCz, FC1, FC3, C3, C1, Cz, C2, C4, CP4, CP2, CPz, CP1, CP3, P3, P1, Pz, P2, P4, PO4, POz, PO3). Electrodes were initially referenced online to the Cz electrode. Separate electrodes were placed on mastoids, to which signal was referenced after recording. The vertical electro-oculogram (EOG) was recorded with two electrodes placed below and above the right eye. The horizontal EOG was recorded from electrodes at the outer canthi of the eyes. The raw EEG signal was 1 Hz high-pass filtered with the default EEGLAB filter: one-pass non-causal zero-phase Hamming-windowed sinc FIR. Time windows of the filtered signal which contained heavy artifacts that could disrupt Independent Component Analysis (ICA) were removed. No channels were removed due to noise. ICA components representing evident artifacts, such as eye blinks, eye movements, and muscular artifacts were removed for each subject (M = 8.24, SD = 2.66). Finally, the average reference was applied.

2.3. Latent fluid intelligence factor

After the EEG recording, four paper-and-pencil *gf* tests were administered. Due to a very weak correlation with the RAPM and the other three remaining tests, one task (Anagrams) was discarded (Table 1). The figural Analogies Test (*Analogies*) included 36 figural analogies in the form "A is to B as C is to X", where simple geometrical patterns A and B were linked according to two to five latent rules (symmetry, rotation, size, color, thickness, number of objects, etc.). The task was to choose one pattern (X) from a selection of four alternative responses that was linked in the same way to pattern C. The Number Series Test (*Numbers*), specifically designed for the study, included 26 items increasing in difficulty, composed by series or 2-D patterns of numbers fulfilling a hidden arithmetic rule. Random position(s) within each item had to be filled in with from one to four missing numbers that correctly completed the series. The Figural Matrices Test (*Figures*), also specifically designed for the study, conceptually corresponded to the *RAPM*. The test included 26 figural patterns (items) in various layouts. For each pattern, a small section was missing, and the participant's task was to choose the section that correctly completed the pattern among four to seven response options. Thirty minutes were given to solve each test. Example items are shown in Fig. 2. Exploratory factor analysis (EFA), which aimed to filter out variance unrelated to the true *gf* variance, used the proportions of correct responses in *RAPM*, *Analogies*, *Numbers*, and *Figures* to generate one *gf* factor that explained 59.3% of total variance in the four test scores (Eigenvalue = 2.37; for factor loadings see Table 1). Each *gf* factor value approximated the intelligence level of a respective participant.

Table 1
Descriptive statistics, reliabilities, and Pearson correlations for all intelligence scores used to compute the *gf* factor (N = 50). All correlations (r) were significant at $p < 0.005$ level.

Statistic\intelligence score	RAPM	Analogies	Numbers	Figures	*gf* factor
Mean	0.623	0.738	0.500	0.443	0.000
SD	0.163	0.160	0.140	0.143	1.000
Min	0.121	0.194	0.077	0.192	− 2.286
Max	0.909	0.972	0.808	0.731	1.953
Skew	− 0.441	− 1.458	− 0.418	− 0.049	− 0.370
Kurtosis	0.526	2.363	0.969	− 0.969	− 0.218
Alpha	0.809	0.840	0.706	0.680	N/A
r(*gf* factor)	0.746	0.775	0.767	0.792	
r(Figures)	0.426	0.469	0.530		
r(Numbers)	0.404	0.429			
r(Analogies)	0.487				

2.4. The strength of phase-amplitude coupling

In order to reliably and comprehensively assess the interplay between fast and slow neuronal oscillations at high spectral resolution, we developed a new method of quantifying the PAC strength for a wide range of frequencies. The method searched for trait-like indices (i.e. reliably identified over the different EEG recordings) of coupling strength among combinations of slow wave phase and fast oscillation amplitude. Consecutive indices were then correlated with the *gf* factor, in order to identify those frequency bands which yielded PAC strongly contributing to individual differences in *gf* (for a graphical illustration of the PAC analysis see Fig. 3). All the analyses were performed in Python using the freely available SciPy, PacPy, and MNE libraries. Specifically, phase information was extracted from 19 "low" frequency EEG bands ranging from 2 to 16 Hz, whereas power amplitude was calculated for 25 "high" frequency ranging between 4 and 64 Hz (Fig. 3A–3C). The center of each frequency band increased in log space. The width of each band was a function of its center frequency (Aru et al., 2015), which was set to ⅛ of the low frequency and to ¼ of the high frequency. We used FIR filters with transition bandwidth of 1 Hz and length corresponding to 2 s, and computed the Hilbert transform of this signal. Its angle was used as the phase time series for low-frequency bands, whereas its real value (signal envelope) served as the amplitude time series for high-frequency bands. The signal in each band was divided into 4-s epochs. For each *RAPM* trial, we used 13 epochs with 2-s overlap, starting 2 s after matrix presentation, and ending 2 s before the response options appeared on the screen. For *Transitive* trials, we used 4 epochs with 1-s overlap, starting 0.5 s after letter pairs presentation, and ending 0.5 s before response options appeared. For *Rest*, we used 89 epochs with 2-s overlap, but later collapsed consecutive epoch triplets into 30 new epoches in order to approximate the numbers of *RAPM* and *Transitive* items.

The strength of PAC between two bands was quantified for each electrode and each epoch separately using a general linear model (GLM) (Penny, Duzel, Miller, & Ojemann, 2008), which define PAC strength as the proportion of variance in amplitude explained by the best-fitting GLM which used sine and cosine of phase as predictors (for illustration of strong, moderate, and weak PAC, see Fig. 3D). As the mean PAC weakens with an increasing modulated frequency (more full

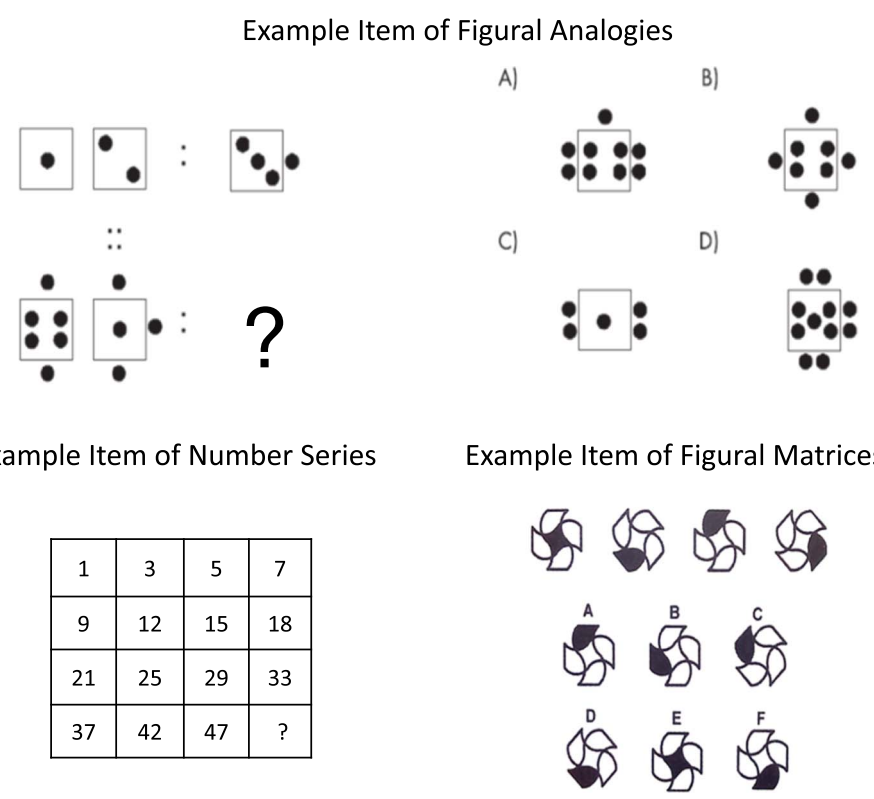

Fig. 2. Example items of the three fluid intelligence tests used to calculate the *gf* factor.

cycles fit in one epoch), the resulting PAC strength for particular pairs of bands was normalized: 100,000 surrogate PAC strength values (from epochs randomly mixed) were generated, and actual PAC strength values were divided by the standard deviation of such a surrogate distribution (i.e., *Z*-scores were calculated). As a result, for each electrode and each epoch we generated *PAC matrix* of normalized PAC strengths, sized 25 (higher frequency bands) × 19 (lower frequency bands), with meaningful PAC strength values defined only for entries for which the frequency of modulated amplitude at least doubled the frequency of modulating phase (i.e., upper triangle of the matrix; see Fig. 3E).

As the particular entry values strongly correlated among the majority of the 34 tested electrodes, and show small variabiliy between epochs, we reduced the number of PAC matrices according to the following procedure. First, for each participant we averaged epochs over trials, resulting in (for each electrode) 34 PAC matrices for *RAPM* and *Transitive*, and 30 in *Rest*. Next, we reduced data across electrodes.

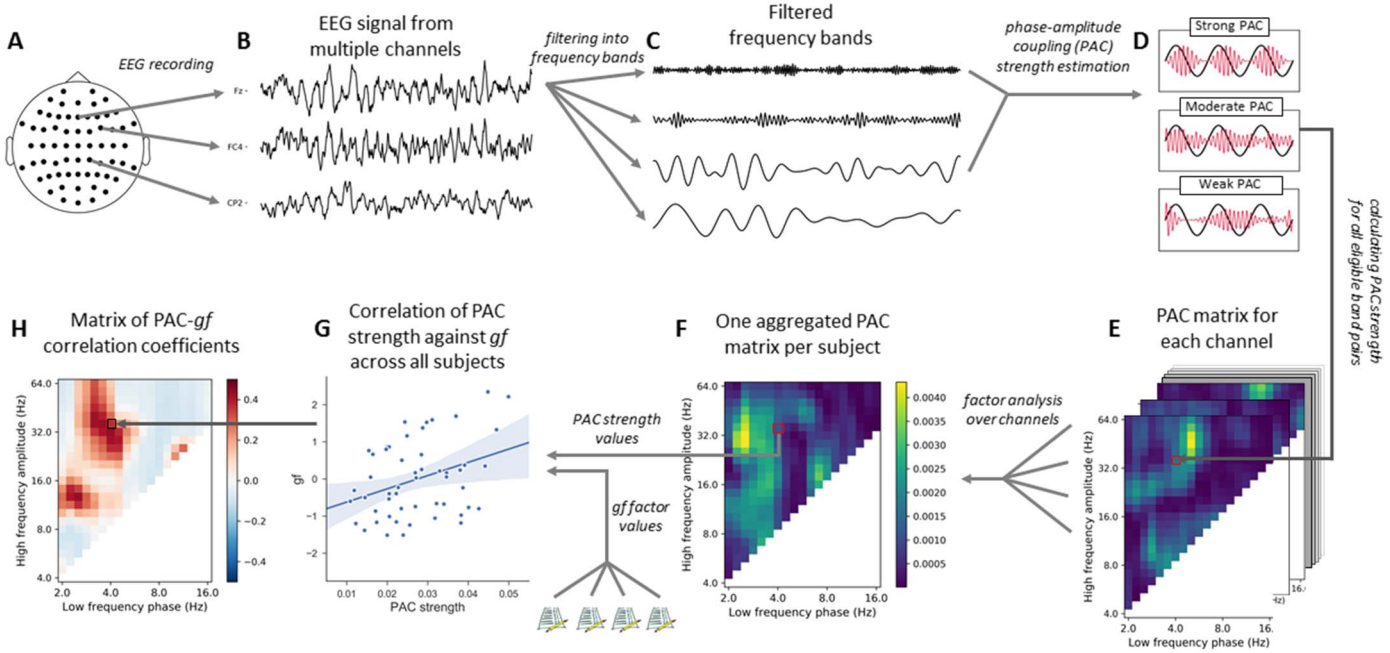

Fig. 3. Main steps of the EEG data analysis. The signal from each EEG channel was filtered (A-C) according to different frequency bands, and the PAC estimated for different frequency combinations (D). Whole brain PAC values across the electrode array (E-F) were then correlated with latent-factor gf scores (G-H).

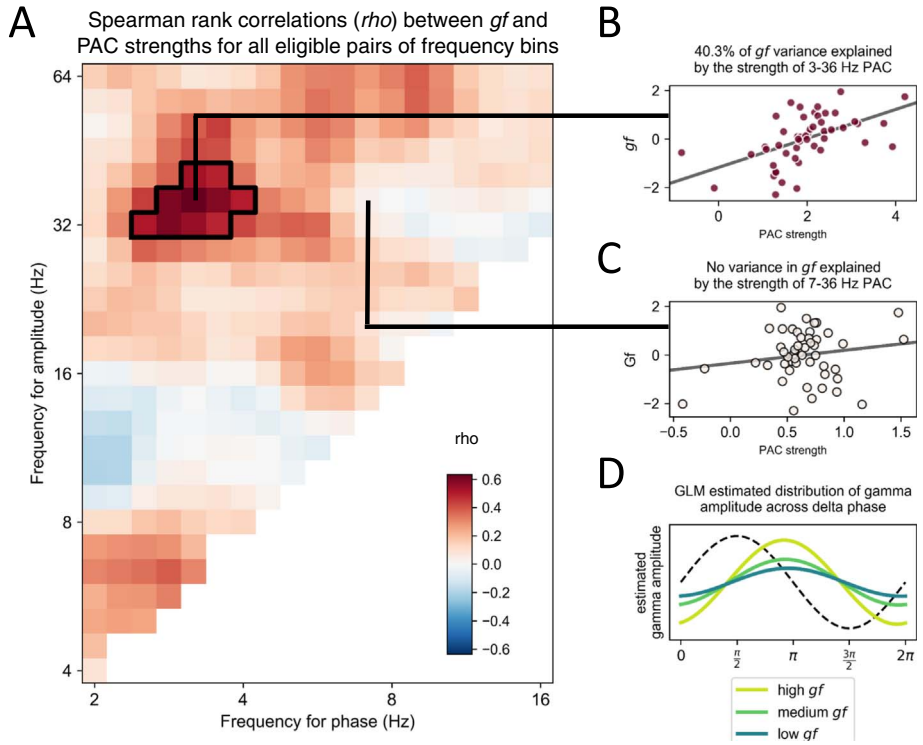

Fig. 4. PAC-*gf* correlation. (A) The matrix displaying the Spearman rank correlation coefficients (*rho*) between the latent *gf* factor and the PAC strength between the phase of low frequency bands (x axis) and the amplitude in higher frequency bands (y axis). Delta-gamma bands inside the black contour predict *gf* at $p_{corr} < 0.05$. (B) *gf* is most strongly predicted by the individual strengths of PAC between the phase of ≈ 3 Hz rhythm and amplitude of ≈ 36 Hz oscillations. (C) PAC strength for all the frequency pairs outside the delta-gamma intersection did not correlate with *gf*. (D) The distribution of 36-Hz amplitude within a 3-Hz cycle estimated by GLM separately for low-, medium- and high-*gf* participants. The higher *gf*, the stronger grouping of the 36-Hz amplitude within the descending phase of 3-Hz oscillation.

However just averaging matrices from our 34 electrodes was not an optimal strategy, because various electrodes differently contributed to the grand-PAC effect (some yielded PAC patterns unrelated to the global PAC pattern). So, an EFA was performed separately for each pair of frequency bands, resulting in one value representing the coupling strength factor for this pair, along with the vector of factor loadings corresponding to the contribution of each electrode to that factor. The EFA approach to data aggregation was chosen over a simple arithmetic mean (which nonetheless yielded comparable results) because the former method produces more reliable effects due to its ability to exclude noisy electrodes by assigning them low factor loadings. In order to avoid unreliable patterns of electrode loadings provided by the EFA, electrode loadings which differed from average loadings by more than two standard deviations were replaced by average loadings for that band. Since (i) the number of to-be-reduced variables (34 electrodes) would be equal to the number of input data points (34 test items, or 30 "items" in case of *Rest*), and (ii) the PAC matrices were smooth (neighboring cells differed little), for each pair of bands we used PAC strengths from surrounding pairs of bands. The resulting vector of 34 (30 in *Rest*) PAC factor values was averaged across the test/Rest items into a single PAC strength value for each pair of bands, which altogether constituted one final PAC matrix for a given EEG measurement (*RAPM*, *Transitive*, *Rest*) and participant (Fig. 3F). Each of these matrices represented a given participant's general index of the non-random synchronization of transient increases in the amplitude of high frequency oscillations happening at specific phases of a slow frequency cycle.

Finally, the Spearman rank correlation *rho* ($N = 50$, $df = 48$) between the *gf* factor and the PAC strength from each cell in the PAC matrix was computed (Fig. 3G). Correction for multiple comparisons was performed via permutation tests, assessing the probability that correlation of equal or higher strength than the observed one could occur by chance. Each permutation consisted of randomly shuffling PAC-*gf* pairs. The resulting matrix reflected the correlations between *gf* and PAC strength for all eligible combinations of slow and high frequency pairs (Fig. 3H).

3. Results

3.1. PAC-gf correlation

Across all possible combinations, significant correlations were found only for the phase of delta oscillations and the amplitude of low gamma activity. The strongest effects were *rho* = 0.480 ($p_{corr} = 0.026$) in *RAPM* (for the 3.1–35.9 Hz pair), *rho* = 0.376 ($p_{corr} = 0.303$) for *Transitive* (3.1–32.0 Hz) and *rho* = 0.509 ($p_{corr} = 0.019$) for *Rest* (2.8–32.0 Hz). A non-significant outcome for *Transitive* might have resulted from the fact that EEG recordings available for this task were shorter. PAC obtained by averaging over *RAPM*, *Transitive*, and *Rest* (with weights reflecting their relative length of EEG signal) yielded strong correlations with *gf* for the 3.1–35.9 Hz pair (*rho* = 0.635, $p_{corr} < 0.001$) and the neighboring delta frequencies (Fig. 4A, B), but not for any other low frequency (Fig. 4C). The GLM parameters that were analyzed separately for three groups of participants defined by the 33% and 66% percentile in the *gf* factor indicated that high-*gf* participants displayed a greater 36-Hz amplitude around the descending phase of 3-Hz delta waves, as compared to medium- and low-*gf* individuals whose gamma amplitude was more evenly dispersed across delta phase (Fig. 4D).

The robustness of the PAC-*gf* link was supported by a leave-one-out cross-validation procedure, a widely accepted method aimed at a conservative estimation of effect size (Picard & Cook, 1984). An iterative procedure set aside a single participant as a test set, and used the PAC matrices of the remaining participants as a training set. Separately for each EEG measurement (i.e., *RAPM*, *Transitive*, and *Rest*), a frequency pair was selected for which the PAC strength most strongly predicted the *gf* factor values of these 49 people. Next, the three vectors of PAC strength values were submitted to a support vector machine (SVM; Vapnik, Golowich, & Smola, 1997) in order to fit the model in which these values altogether better predicted the *gf* factor. Finally, the model predicted the *gf* factor value of the one participant left out. After 50 iterations, the SVM yielded 50 predicted *gf* values of participants left out during each training step. For all 50 pairs selected in the cases of *RAPM* and *Rest*, respectively, the low frequency fell within the 3-5 Hz

range (delta), and the high frequency was within the 32-40 Hz range (low gamma). In the case of *Transitive*, 40 pairs fitted these two ranges. The dominant pair was the 3–36 Hz. Finally, the predicted *gf* factor values could be correlated with the real *gf* factor values of participants. The resulting Spearman rank correlation of *rho* = 0.593 (35.1% shared variance; $p < 0.0001$) suggested that the effect of the 3-36 Hz PAC strength on *gf* is sufficiently robust, and would likely generalize in bigger samples.

3.2. Comparison with other gf markers

Additionally, the 3–36 Hz PAC's unique contribution to individual variability in *gf* was validated against six previously identified frequency-domain electrophysiological predictors of *gf*. The predictors included Higuchi (1988) fractal dimension (*d*; a measure of complexity of the individual raw EEG signal), the spectral power for each band (the strength of given oscillatory frequency; see Jaušovec & Jaušovec, 2000; Keizer, Verschoor, Verment, & Hommel, 2010), theta and alpha individual peak frequency (the frequency of spectral peak within a specific oscillatory band; Grandy et al., 2013; Jaušovec & Jaušovec, 2000), the within-frequency coupling measured with global synchrony (Stankov et al., 2006) and phase-locking (Sauseng, Klimesch, Schabus, & Doppelmayr, 2005), as well as the AAC strength (Hipp, Hawellek, Corbetta, Siegel, & Engel, 2012; Pahor & Jaušovec, 2014a, 2014b). Specifically, global synchrony was calculated as the circular variance of oscillatory phase among multiple electrodes (with low variance meaning high synchrony; Stankov et al., 2006). Phase coherence was calculated for the parieto-frontal electrode pairs as the stability (the larger the better) of frequency-specific phase difference between selected pairs of channels (Palva, Monto, Kulashekhar, & Palva, 2010). The AAC strength was calculated analogously as the PAC strength, with the sole exception that, instead of sine and cosine of phase, the amplitude of low frequency signal was used as a predictor in GLM. When aggregated over *Rest*, *RAPM*, and *Transitive*, all those indexes provided lower predictive values over *gf* (all *rhos* < 0.32; Table 2 and Fig. 5), as compared to the 3–36 Hz PAC.

3.3. Dynamic and topography of PAC-gf

Finally, to confirm that the 3–36 Hz PAC was related to increased reasoning effort, we compared the gamma amplitude concentration around the phase of delta between *RAPM*, *Transitive*, and *Rest*. Specifically, we approximated the distribution of the high band amplitude over the low band phase across all epochs by looking at the GLM estimates of the angular degree within the phase at which the amplitude's maximum occurred. The resulting degree was corrected for dipolarity (the phases for opposite poles of a dipolar source were reversed). The resulting distributions (Fig. 6A) indicate a stronger gamma amplitude concentration around descending delta phase during *RAPM* and *Transitive* than in *Rest* (both *ps* < 0.0001; *t*-test for deviations from circular mean). Moreover, the PAC strength decreased during solution of each *RAPM* items (Fig. 6B), as shown by the Page (1963) test, $p < 0.001$. Consistently, topographic analyses indicated that, comparing to central EEG recording sites, the PAC-*gf* correlation was more pronounced at the midline frontal ($Z_{(48)} = 1.64$, $p = 0.052$) and parietal ($Z_{(48)} = 2.78$, $p = 0.003$) EEG electrodes (Fig. 6C). These sites were previously identified using fMRI and PET data as the key foci of reasoning and problem solving, according to the parieto-frontal integration theory (P-FIT) (Jung & Haier, 2007). No significant *rho* was found in lateral sites, and, generally, PAC was weak at these sites.

4. Discussion

The present investigation of the correlation between *gf* and PAC strengths for slow and fast oscillatory bands revealed one potential candidate related to the coupling of delta and gamma oscillations. Such specific phase-amplitude interaction explained 35% of variance in the *gf* factor derived from four different intelligence tests, according to a cross-validated regression model. Although previous studies (e.g., Leszczynski et al., 2015; Roux & Uhlhaas, 2014; Sauseng et al., 2009; Voytek et al., 2010) suggested that individual differences in cognitive performance, especially at working memory tasks, can be linked to oscillations ranging from 6 (theta) to 12 Hz (alpha), our finding suggest that slower oscillations in the delta band also contribute to individual variance in higher order cognition. Our results are coherent with existing views that fluid reasoning, although being strongly dependent on working memory, constitutes a more complex and diverse cognitive process, occurring at slower pace than required for typical working memory operations (Carpenter et al., 1990; Chuderski & Andrelczyk, 2015; Johnson-Laird, 2006; Knowlton et al., 2012). The weakened delta-gamma PAC observed in our data at later stages of *RAPM* trials solutions (i.e. when participants are more likely to have identified the correct solution while still maintaining information in working memory), supports this view. Interestingly, although gamma amplitude during *Rest* was less strongly coupled with the descending delta phase than during reasoning tests, it equally predicted the *gf* factor, in line with a recent study suggesting that organization of spontaneous functional activity of intelligent brains strongly resembles their activity during demanding cognitive tasks (Schultz & Cole, 2016). Furthermore, although EEG studies are generally sub-optimal for deriving topographical information about cognitive processes, the relatively larger *gf*-PAC strength observed in medial frontal and parietal electrodes

Table 2
Spearman correlations between the *gf* factor, PAC strength, and six alternative EEG predictors of *gf*. Maximal *rho* values are shown for a EEG measurement (i.e., *RAPM*, *Transitive*, or *Rest*) most strongly predicting *gf*, as well as for the average across the three EEG measurements.

Measure\band	Maximal value of *rho* within the three measurements					Maximal value of *rho* within the three measurements aggregated				
	Delta	Theta	Alpha	Beta	Gamma	Delta	Theta	Alpha	Beta	Gamma
Delta-modulated PAC		0.333	−0.330	−0.263	*0.509*		0.333	−0.331	−0.306	***0.635***
Theta-modulated PAC			0.223	−0.279	0.401			−0.203	0.226	0.356
Alpha-modulated PAC				−0.272	−0.344				−0.243	−0.332
Delta-modulated AAC		−0.395	−0.373	−0.486†	−0.368		0.196	−0.172	−0.255	−0.264
Theta-modulated AAC			−0.189	−0.287	−0.350			−0.189	−0.191	−0.222
Alpha-modulated AAC				0.252	−0.246				−0.172	−0.164
Band power	0.297	0.316	0.100	0.152	0.229	0.303	0.316	0.070	0.127	0.197
Individual peak *f*		0.389	0.363				0.293	0.286		
Global synchrony	−0.129	0.209	−0.241	−0.185	0.121	0.265	0.267	0.277	0.196	0.283
P-F coherence	−0.202	−0.216	0.072	0.139	−0.198	−0.115	−0.134	0.067	0.085	−0.212
Higuchi fractal *d*	0.134					0.104				

Note. Values in regular font are not significant at $p > 0.1$ level (FDR-corrected). † indicates $p = 0.075$. Italicized indicates $p = 0.019$. Bolded italicized indicates $p < 0.001$. Blank space = a given measure cannot be defined for a given band. Higuchi *d* was computed for the total signal.

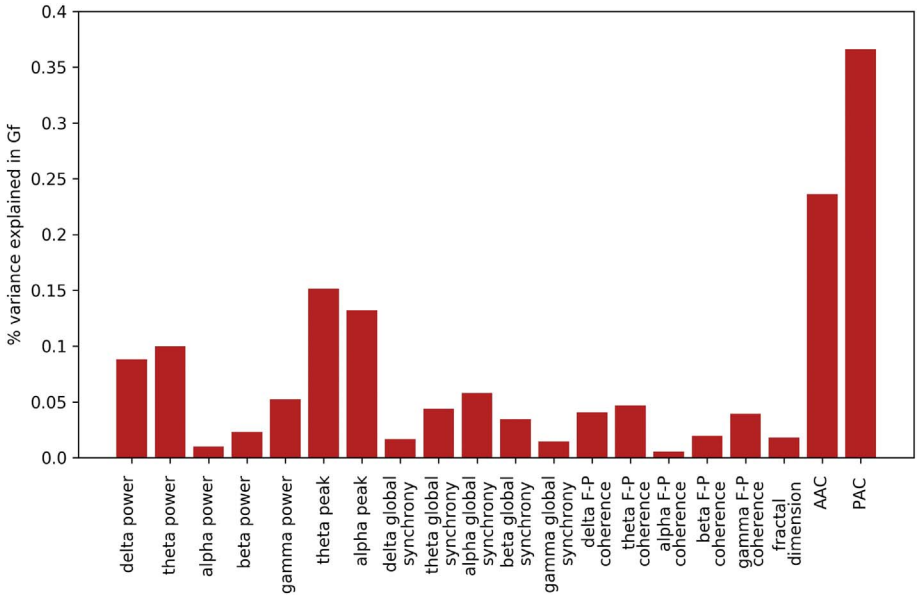

Fig. 5. Maximum percentage of variance in the *gf* factor explained by each alternative EEG-based measure, as compared to 40.3% of variance explained by the 3–36 Hz PAC.

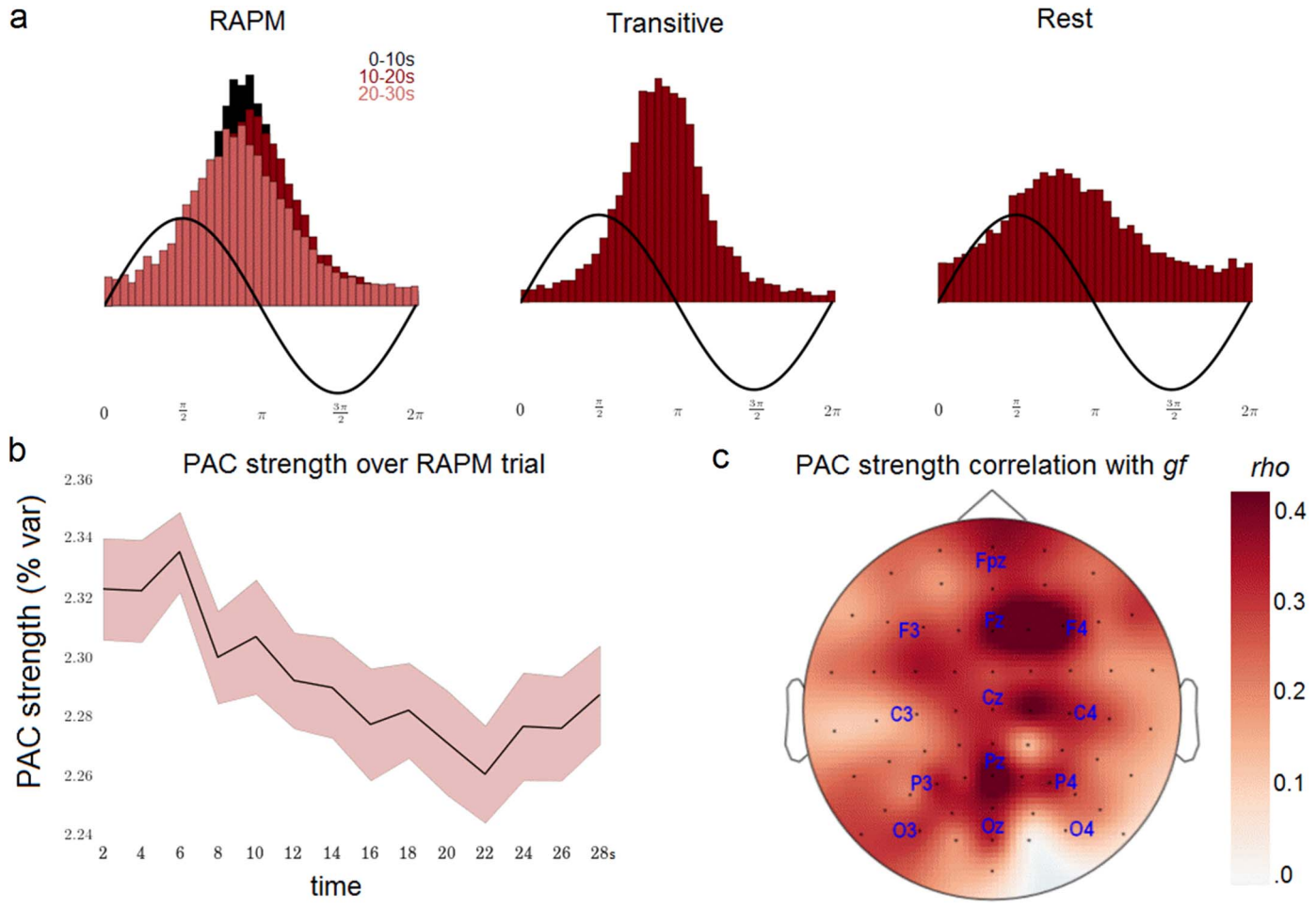

Fig. 6. Dynamic and topography of the PAC. (A) The estimated distribution of the 36-Hz gamma amplitude (red bars) is visibly more concentrated around the descending phase of 3-Hz delta (black sinusoid) in the two *gf* tests (*RAPM* and *Transitive* task), as compared to the resting state. Also, concentration of gamma activity at this specific phase of delta was strongest during the first 10 s of each *RAPM* trial (dark red bars) than in the second (medium red) and the last 10 s (light red), possibly reflecting increased reasoning during the early stages of problem solving. (B) Significant drop in the average PAC strength during solution of *RAPM* trials. The error bar corresponds to one standard deviation estimate using a bootstrap procedure. (C) Scalp topography of Spearman rank correlation values (*rho*) between the average delta-gamma PAC strength in *RAPM* and the latent *gf* factor, showing the strongest effects in the frontal and parietal EEG recording sites.

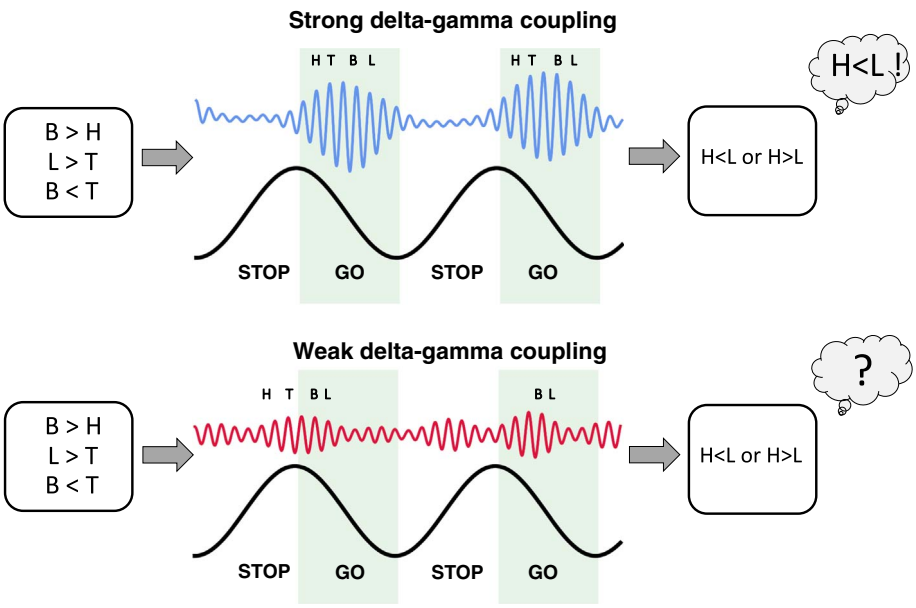

Fig. 7. A possible theoretical explanation of the relationship between the PAC strength and *gf* performance. Delta cycle integrates consecutive elements of e.g. a *Transitive* reasoning problem, which are encoded in working memory by dedicated gamma cycles. As suggested by Leszczynski et al. (2015) these elements can be effectively activated only in the descending delta phase bins ("Go" period), while they are suppressed during the ascending phase bins ("Stop" period). With strong PAC, almost all gamma amplitude is grouped within Go periods, therefore all the elements can be activated. When PAC is weak, gamma oscillations-based encoding of problem's items might fall in Stop periods, thus not being available and likely leading to suboptimal perfomance.

seems coherent with the Parieto-Frontal Integration Theory of neurobiological basis of intelligence (Jung & Haier, 2007), as well as with two recent large-scale meta-analyses of neuroimaging data (Basten et al., 2015; Santarnecchi et al., 2017). Finally, delta-gamma PAC showed higher explanatory power over *gf* than six other EEG-based measures pertaining to complexity, spectral power, individual peak-frequency, spectral coherence, synchrony, and AAC.

We interpret the delta-gamma PAC as the neurophysiological substrate behind the integration of consecutive elements during *gf* test problem-solving. Existing studies in non-human primates (Naya & Suzuki, 2011; Siegel et al., 2009) and computer simulations (Chuderski & Andrelczyk, 2015; Horn & Usher, 1991; Knowlton et al., 2012; Lisman & Idiart, 1995; Vogel et al., 2001) suggest that such elements are encoded in working memory by separate burst of gamma oscillations, while a recent human intracranial study (Leszczynski et al., 2015) indicates that such oscillations can be active only in the descending delta phase ("Go" period), but are suppressed during the ascending phase of delta ("Stop" period). In a *gf* task, local gamma oscillations might represent the key for features binding, with the precise synchronization to Go phase bins of the delta cycle may be crucial for effective maintenance of such information over time (for a schematic example concerning the transitive reasoning task see Fig. 7). A larger gamma activity during Go periods will result in a larger probability that the crucial features of the problem will be effectively encoded, resulting in higher probability of a correct response. More gamma activation in Stop periods will lead to some elements vanishing from working memory, that might cause errors or guessing during *gf* testing. Interestingly, such link between delta-gamma PAC and *gf* seems to be supported by their shared developmental trajectory (Cho et al., 2015), i.e. both visibly drop by the age of 20.

One potential limitation of the present study resides in the still limited understanding of the neurophysiological nature and substrate of PAC, which involve many alterative theoretical and computational models (e.g., Jirsa & Müller, 2013; Onslow, Jones, Bogacz, & Tort, 2014). As EEG data reflects transcranial and highly aggregated echo of neuronal activity, PAC patterns observed in EEG signals are likely rooted in some unknown brain processes, which can actually determine a chain of events across the micro-, meso- and macro-scale leading to quantifiable individual differences in human intelligence levels. Any future findings regarding such mechanisms (e.g., coming from invasive recording as those obtained via ECoG) may impose revisions to our model of the PAC-*gf* relationship. Furthermore, some researchers suggest that PAC may reflect spurious coupling (accidental synchrony) resulting from activation bursts (e.g., after stimulus presentation; Sauseng et al., 2007) and non-sinusoidal shapes of EEG waves (Cole & Voytek, 2017). Although the present data do not allow for definite exclusion of such hypotheses, we made extensive efforts to minimize its likelihood: we (i) analyzed EEG data from three separate measurements (both resting activity and reasoning tasks), yielding as much as over 20 min of signal per participant, we (ii) left out signal directly succeeding the stimulus presentation, we (iii) normalized data where possible, we (iv) consecutively used permutation tests, and we (v) followed other recommendations aimed at avoiding artifacts that generate spurious PAC (Aru et al., 2015).

Another potential limitation concerns the origins of gamma activity itself, as observed in our data during *gf*-related cognitive processing. One could argue that such gamma activity is not of neural origin but constitutes a spectral fingerprint of (micro)saccades (Bosman, Womelsdorf, Desimone, & Fries, 2009; Yuval-Greenberg, Tomer, Keren, Nelken, & Deouell, 2008). Following this logic, the modulation of gamma frequency by delta phase could result from microsaccades occurring at 3 to 4 Hz (e.g., Lowet, Roberts, Bosman, Fries, & De Weerd, 2016). However, such an 'ocular' interpretation of our results seems unlikely for multiple reasons. For instance, such PAC-*gf* correlation was observed also for resting-EEG data during eyes closed condition, which unlikely yielded regular eye movements. Moreover, if the delta-gamma coupling was of ocular origin, a different topography should have been observed (see Fig. 6C). Finally, according to Hipp and Siegel (2013), the independent component analysis (ICA)-based preprocessing method applied on our data is thought of removing any muscular and microsaccadic artifact from the EEG signal. Nonetheless, future studies should investigate this hypothesis with ad-hoc data collection including EEG and eye-tracking data.

In summary, we provided a novel evidence of a potential neurophysiological oscillatory mechanism significantly contributing to human fluid intelligence perfomance. More in-depth analysis of delta-gamma PAC might help explain cognitive deficits commonly observed in neurological and psychiatric conditions (Günetkin & Başar, 2016), as well as guide recent cognitive enhancement interventions based on entrainment of endogenous oscillatory activity via non-invasive brain stimulation (e.g., Pahor & Jaušovec, 2014a; Polania, Nitsche, Korman, Batsikadze, & Paulus, 2012; Santarnecchi et al., 2016; see Jaušovec & Pahor, 2017; Santarnecchi et al., 2015).

Acknowledgments

The raw EEG and behavioral data can be downloaded from: https://www.dropbox.com/sh/55drru0yv28xavl/AAAeEP6JEb0Vt0ZunwfWWFyqa?dl=0.

The python code used for the analysis is available upon request to the corresponding author. This study was supported by Foundation for Polish Science (the MISTRZ grant no. 3/2015 sponsored to Adam Chuderski). Dr. Santarnecchi is partially supported by the Office of the Director of National Intelligence (ODNI) and Intelligence Advanced Research Projects Activity (IARPA), via grant no. 2014-13121700007. The views and conclusions contained herein are those of the authors and should not be interpreted as necessarily representing the official policies or endorsements, either expressed or implied, of the ODNI, IARPA, or the U.S. Government. Dr. Santarnecchi is supported by the Beth Israel Deaconess Medical Center (BIDMC) via the Chief Academic Officer (CAO) grant 2017 no. 60182, and the Defense Advanced Research Projects Agency (DARPA) via grant no. HR001117S0030. The authors declare no conflict of interests.

References

Aru, J., et al. (2015). Untangling cross-frequency coupling in neuroscience. *Current Opinion in Neurobiology, 31*, 51–61. http://dx.doi.org/10.1016/j.conb.2014.08.002.

Axmacher, N., Henseler, M. M., Jensen, O., Weinreich, I., Elger, C. E., & Fell, J. (2010). Cross-frequency coupling supports multi-item working memory in the human hippocampus. *PNAS, 107*, 3228–3233.

Barbey, A. K., Colom, R., Paul, E. J., & Grafman, J. (2014). Architecture of fluid intelligence and working memory revealed by lesion mapping. *Brain Structure & Function, 219*(2), 485–494. http://dx.doi.org/10.1007/s00429-013-0512-z.

Basten, U., Hilger, K., & Fiebach, C. J. (2015). Where smart brains are different: A quantitative meta-analysis of functional and structural brain imaging studies on intelligence. *Intelligence, 51*, 10–27.

Bosman, C. A., Womelsdorf, T., Desimone, R., & Fries, P. (2009). A microsaccadic rhythm modulates gamma-band synchronization and behavior. *Journal of Neuroscience, 29*, 9471–9480.

Canolty, R. T., & Knight, R. T. (2010). The functional role of cross-frequency coupling. *Trends in Cognitive Sciences, 14*(11), 506–515. http://dx.doi.org/10.1016/j.tics.2010.09.001.

Canolty, R. T., et al. (2006). High gamma power is phase-locked to theta oscillations in human neocortex. *Science, 313*(5793), 1626–1628. http://dx.doi.org/10.1126/science.1128115.

Carpenter, P. A., Just, M. A., & Shell, P. (1990). What one intelligence test measures: A theoretical account of the processing in the Raven Progressive Matrices Test. *Psychological Review, 97*(3), 404–431.

Cho, R. Y., et al. (2015). Development of sensory gamma oscillations and cross-frequency coupling from childhood to early adulthood. *Cerebral Cortex, 25*(6), 1509–1518. http://dx.doi.org/10.1093/cercor/bht341.

Chuderski, A. (2013). When are fluid intelligence and working memory isomorphic and when are they not? *Intelligence, 41*, 244–262.

Chuderski, A., & Andrelczyk, K. (2015). From neural oscillations to reasoning ability: Simulating the effect of the theta-to-gamma cycle length ratio on individual scores in a figural analogy test. *Cognitive Psychology, 76*, 78–102. http://dx.doi.org/10.1016/j.cogpsych.2015.01.001.

Clayden, J. D., Jentscke, S., Muñoz, M., Cooper, J. M., Chadwick, M. J., & Banks, T. (2012). Normative development of white matter tracts: Similarities and differences in relation to age, gender and intelligence. *Cerebral Cortex, 22*, 1738–1747.

Cole, M. W., Yarkoni, T., Repovs, G., Anticevic, A., & Braver, T. S. (2012). Global connectivity of prefrontal cortex predicts cognitive control and intelligence. *Journal of Neuroscience, 32*(26), 8988–8999. http://dx.doi.org/10.1523/JNEUROSCI.0536-12.2012.

Cole, S. R., & Voytek, B. (2017). Brain oscillations and the importance of waveform shape. *Trends in Cognitive Sciences, 21*, 137–149.

Colom, R., Burgaleta, M., Roman, F. J., Karama, S., Alvarez-Linera, J., Abad, F. J., et al. (2013). Neuroanatomic overlap between intelligence and cognitive factors: Morphometry methods provide support for the key role of the frontal lobes. *NeuroImage, 72*, 143–152.

Colom, R., Haier, R. J., Head, K., Álvarez-Linera, J., Quiroga, M.Á., Shih, P. C., et al. (2009). Graymatter correlates of fluid, crystallized, and spatial intelligence: Testing the P-FIT model. *Intelligence, 37*, 124–135.

Colom, R., Karama, S., Jung, R. E., & Haier, R. J. (2010). Human intelligence and brain networks. *Dialogues in Clinical Neuroscience, 12*, 489–501.

Cowan, N. (2001). The magical number 4 in short-term memory: A reconsideration of mental storage capacity. *Behavioral and Brain Sciences, 24*, 87–185.

Deary, I. J. (2012). Intelligence. *Annual Review of Psychology, 63*, 453–482. http://dx.doi.org/10.1146/annurev-psych-120710-100353.

Deary, I. J., Penke, L., & Johnson, W. (2010). The neuroscience of human intelligence differences. *Nature Reviews Neuroscience, 11*(3), 201–211.

Dunst, B., et al. (2014). Neural efficiency as a function of task demands. *Intelligence, 42*, 22–30.

Eliasmith, C., et al. (2012). A large-scale model of the functioning brain. *Science, 338*(6111), 1202–1205. http://dx.doi.org/10.1126/science.1225266.

Finn, E. S., et al. (2015). Functional connectome fingerprinting: Identifying individuals using patterns of brain connectivity. *Nature Neuroscience, 18*(11), 1664–1671.

Grandy, T. H., Werkle-Bergner, M., Chicherio, C., Lovden, M., Schmiedek, F., & Lindenberger, U. (2013). Individual alpha peak frequency is related to latent factors of general cognitive abilities. *NeuroImage, 79*, 10–18. http://dx.doi.org/10.1016/j.neuroimage.2013.04.059.

Günetkin, B., & Başar, E. (2016). Review of evoked and event-related delta responses in the human brain. *International Journal of Psychophysiology, 103*, 22–42. http://dx.doi.org/10.1016/j.ijpsycho.2015.02.017.

Higuchi, T. (1988). Approach to an irregular time series on the basis of the fractal theory. *Physica D: Nonlinear Phenomena, 31*(2), 277–283.

Hipp, J. F., Hawellek, D. J., Corbetta, M., Siegel, M., & Engel, A. K. (2012). Large-scale cortical correlation structure of spontaneous oscillatory activity. *Nature Neuroscience, 15*(6), 884–890. http://dx.doi.org/10.1038/nn.3101.

Hipp, J. F., & Siegel, M. (2013). Dissociating neuronal gamma-band activity from cranial and ocular muscle activity in EEG. *Frontiers in Human Neuroscience, 7*.

Horn, D., & Usher, M. (1991). Parallel activation of memories in an oscillatory neural network. *Neural Computation, 3*(1), 31–43.

Jaušovec, N., & Jaušovec, K. (2000). Differences in resting EEG related to ability. *Brain Topography, 12*(3), 229–240.

Jaušovec, N., & Pahor, A. (2017). *Increasing intelligence*. London, UK: Academic Press.

Jensen, O., & Colgin, L. L. (2007). Cross-frequency coupling between neuronal oscillations. *Trends in Cognitive Sciences, 11*, 267–269.

Jirsa, V., & Müller, V. (2013). Cross-frequency coupling in real and virtual brain networks. *Frontiers in Computational Neuroscience, 7* (Article 78).

Johnson-Laird, P. N. (2006). *How we reason*. New York: Oxford University Press.

Jung, R. E., & Haier, R. J. (2007). The Parieto-Frontal Integration Theory (P-FIT) of intelligence: Converging neuroimaging evidence. *Behavioral and Brain Sciences, 30*(2), 135–154. http://dx.doi.org/10.1017/S0140525X07001185.

Kane, M. J., Hambrick, D. Z., & Conway, A. R. A. (2005). Working memory capacity and fluid intelligence are strongly related constructs: Comment on Ackerman, Beier, and Boyle (2005). *Psychological Bulletin, 131*, 66–71.

Keizer, A. W., Verschoor, M., Verment, R. S., & Hommel, B. (2010). The effect of gamma enhancing neurofeedback on the control of feature bindings and intelligence measures. *International Journal of Psychophysiology, 75*(1), 25–32. http://dx.doi.org/10.1016/j.ijpsycho.2009.10.011.

Knowlton, B. J., Morrison, R. G., Hummel, J. E., & Holyoak, K. J. (2012). A neurocomputational system for relational reasoning. *Trends in Cognitive Sciences, 16*(7), 373–381. http://dx.doi.org/10.1016/j.tics.2012.06.002.

Leszczynski, M., Fell, J., & Axmacher, N. (2015). Rhythmic working memory activation in the human hippocampus. *Cell Reports, 13*(6), 1272–1282. http://dx.doi.org/10.1016/j.celrep.2015.09.081.

Lisman, J. E., & Idiart, M. A. (1995). Storage of 7 ± 2 short-term memories in oscillatory subcycles. *Science, 267*(5203), 1512–1515.

Lisman, J. E., & Jensen, O. (2013). The theta-gamma neural code. *Neuron, 77*, 1002–1016.

Lowet, E., Roberts, M. J., Bosman, C. A., Fries, P., & De Weerd, P. (2016). Areas V1 and V2 show microsaccade-related 3–4-Hz covariation in gamma power and frequency. *European Journal of Neuroscience, 43*, 1286–1296.

McGrew, K. S. (2009). CHC theory and the Human Cognitive Abilities Project: Standing on the shoulders of the giants of psychometric intelligence research. *Intelligence, 37*, 1–10.

Naya, Y., & Suzuki, W. A. (2011). Integrating what and when across the primate medial temporal lobe. *Science, 333*(6043), 773–776. http://dx.doi.org/10.1126/science.1206773.

Neubauer, A. C., & Fink, A. (2009). Intelligence and neural efficiency. *Neuroscience and Biobehavioral Reviews, 33*(7), 1004–1023. http://dx.doi.org/10.1016/j.neubiorev.2009.04.001.

Onslow, A. C., Jones, M. W., Bogacz, R., & Tort, A. B. (2014). A canonical circuit for generating phase-amplitude coupling. *PLoS ONE, 9*, e102591.

Othani, T., et al. (2014). Medial frontal white and gray matter contributions to general intelligence. *PLoS One, 9*, e2691.

Page, E. B. (1963). Ordered hypotheses for multiple treatments: A significance test for linear ranks. *Journal of the American Statistical Association, 58*(301), 216–230.

Pahor, A., & Jaušovec, N. (2014a). The effects of theta transcranial alternating current stimulation (tACS) on fluid intelligence. *International Journal of Psychophysiology, 93*, 322–331.

Pahor, A., & Jaušovec, N. (2014b). Theta–gamma cross-frequency coupling relates to the level of human intelligence. *Intelligence, 46*, 283–290.

Palva, J. M., Monto, S., Kulashekhar, S., & Palva, S. (2010). Neuronal synchrony reveals working memory networks and predicts individual memory capacity. *Proceedings of the National Academy of Sciences of the United States of America, 107*(16), 7580–7585. http://dx.doi.org/10.1073/pnas.0913113107.

Penny, W. D., Duzel, E., Miller, K. J., & Ojemann, J. G. (2008). Testing for nested oscillation. *Journal of Neuroscience Methods, 174*(1), 50–61. http://dx.doi.org/10.1016/j.jneumeth.2008.06.035.

Picard, R., & Cook, D. (1984). Cross-validation of regression models. *Journal of the American Statistical Association, 79*, 575–583.

Pineda-Pardo, J. A., Martinez, J., Roman, F. J., & Colom, R. (2016). Structural efficiency within a parietal-frontal network and cognitive differences. *Intelligence, 54*, 105–116.

Polania, R., Nitsche, M. A., Korman, C., Batsikadze, G., & Paulus, W. (2012). The importance of timing in segregated theta phase-coupling for cognitive performance. *Current Biology, 22*(14), 1314–1318. http://dx.doi.org/10.1016/j.cub.2012.05.021.

Ragni, M., & Knauff, M. (2013). A theory and a computational model of spatial reasoning

with preferred mental models. *Psychological Review, 120*(3), 561–588. http://dx.doi.org/10.1037/a0032460.

Roux, F., & Uhlhaas, P. J. (2014). Working memory and neural oscillations: Alpha-gamma versus theta-gamma codes for distinct WM information? *Trends in Cognitive Sciences, 18*, 16–25.

Santarnecchi, E., Muller, T., Rossi, S., Sarkar, A., Polizzotto, N. R., Rossi, A., et al. (2016). Individual differences and specificity of prefrontal gamma frequency-tACS on fluid intelligence capabilities. *Cortex, 75*, 33–43.

Santarnecchi, E., et al. (2015). Enhancing cognition using transcranial electrical stimulation. *Current Opinion in Behavioral Sciences, 4*, 171–178.

Santarnecchi, E., et al. (2017). Dissecting the parieto-frontal correlates of intelligence: A comprehensive ALE meta-analysis study. *Intelligence, 63*, 9–28. http://dx.doi.org/10.1016/j.intell.2017.04.008.

Sauseng, P., Klimesch, W., Gruber, W. R., Hanslmayr, S., Freunberger, R., & Doppelmayr, M. (2007). Are ERP components generated by phase resetting of brain oscillations? A critical discussion. *Neuroscience, 146*, 1435–1444.

Sauseng, P., Klimesch, W., Schabus, M., & Doppelmayr, M. (2005). Fronto-parietal EEG coherence in theta and upper alpha reflect central executive functions of working memory. *International Journal of Psychophysiology, 57*(2), 97–103. http://dx.doi.org/10.1016/j.ijpsycho.2005.03.018.

Sauseng, P., et al. (2009). Brain oscillatory substrates of visual short-term memory capacity. *Current Biology, 19*(21), 1846–1852. http://dx.doi.org/10.1016/j.cub.2009.08.062.

Schultz, D. H., & Cole, M. W. (2016). Higher intelligence is associated with less task-related brain network reconfiguration. *Journal of Neuroscience, 36*(33), 8551–8561. http://dx.doi.org/10.1523/JNEUROSCI.0358-16.2016.

Siegel, M., Warden, M. R., & Miller, E. K. (2009). Phase-dependent neuronal coding of objects in short-term memory. *Proceedings of the National Academy of Sciences of the United States of America, 106*(50), 21341–21346. http://dx.doi.org/10.1073/pnas.0908193106.

Stankov, L., et al. (2006). Intelligence and the tuning-in of brain networks. *Learning and Individual Differences, 16*(3), 217–233.

Szczepanski, S. M., Crone, N. E., Kuperman, R. A., Auguste, K. I., Parvizi, J., & Knight, R. T. (2014). Dynamic changes in phase-amplitude coupling facilitate spatial attention control in fronto-parietal cortex. *PLoS Biology, 12*(8), e1001936. http://dx.doi.org/10.1371/journal.pbio.1001936.

van den Heuvel, M. P., Stam, C. J., Kahn, R. S., & Pol, H. (2009). Efficiency of functional brain networks and intellectual performance. *Journal of Neuroscience, 29*(23), 7619–7624.

van Vugt, M. K., Schulze-Bonhage, A., Litt, B., Brandt, A., & Kahana, M. J. (2010). Hippocampal gamma oscillations increase with memory load. *Journal of Neuroscience, 30*, 2694–2699.

Vapnik, V., Golowich, S. E., & Smola, A. J. (1997). Support vector method for function approximation, regression estimation and signal processing. *Advances in Neural Information Processing Systems, 9*, 281–287.

Vogel, E. K., Woodman, G. F., & Luck, S. J. (2001). Storage of features, conjunctions, and objects in visual working memory. *Journal of Experimental Psychology: Human Perception & Performance, 27*, 92–114.

Voytek, B., Canolty, R. T., Shestyuk, A., Crone, N. E., Parvizi, J., & Knight, R. T. (2010). Shifts in gamma phase–amplitude coupling frequency from theta to alpha over posterior cortex during visual tasks. *Frontiers in Human Neuroscience,* 4 (Article 191).

Watrous, A. J., Deuker, L., Fell, J., & Axmacher, N. (2015). Phase-amplitude coupling supports phase coding in human ECoG. *eLife, 4*, e07886. http://dx.doi.org/10.7554/eLife.07886.

Yuval-Greenberg, S., Tomer, O., Keren, A. S., Nelken, I., & Deouell, L. Y. (2008). Transient induced gamma-band response in EEG as a manifestation of miniature saccades. *Neuron, 58*, 429–441.